J|A|C|S
ARTICLES
Published on Web 12/27/2001

^{67}Zn Solid-State and Single-Crystal NMR Spectroscopy and X-ray Crystal Structure of Zinc Formate Dihydrate

Andrew S. Lipton, Mark D. Smith,† Richard D. Adams,† and Paul D. Ellis*

Contribution from the Macromolecular Structure & Dynamics Directorate, WR Wiley Environmental Molecular Sciences Laboratory, Pacific Northwest National Laboratory, Richland, Washington 99352, and Department of Chemistry and Biochemistry, University of South Carolina, Columbia, South Carolina 29208

Received July 12, 2001

Abstract: The crystal structure, quadrupole coupling parameters, and the orientation of the electric field gradient tensors for each site of zinc formate dihydrate have been determined. There are two distinct sites in the asymmetric unit: one containing four in-plane waters with two bridging formats, the other containing six bridging formates. The solid-state NMR lineshapes have been assigned to their respective sites by using isotopic labeling and cross-polarization methods. The hydrated site corresponds to the lineshape having a quadrupole coupling constant (Cq) of 9.6 MHz and the anhydrous site has a Cq of 6.2 MHz. The absence of chemical shielding contributions to the observed lineshapes has been verified with a high-field solid-state NMR experiment performed at 18.8 T.

Introduction

Recognizing the importance of understanding the nature of the zinc site in metalloproteins, Valley[1] pioneered the surrogate probe strategy by which they replaced the native Zn^{2+} ion with another metal ion, e.g. $Co^{2+/3+}$, with more favorable spectroscopic properties. As a result of this substitution, the UV/vis electronic spectrum or its EPR could be examined as a means to follow the chemistry at the metal site. We[2] and others[3] took this same approach from the perspective of NMR spectroscopy. That is, Cd^{2+} ions were employed as a surrogate probe for Zn^{2+} ions. Cadmium-113 being a spin $^1/_2$ nuclide makes it amenable to all of the standard liquid and solid-state NMR methods. Further, cadmium and zinc have similar chemistries and the divalent metal ions are similar in size (i.e. 0.69 Å for Zn^{2+} and 0.92 Å for Cd^{2+}). However, due to the size differences and the fact that the chemistries are not identical, one should exercise care in utilizing this strategy. The Parkin group has recently noted significant structural differences when constructing analogous models of cadmium and zinc.[4] Given the potential for problems, it is important to note that over the past thirty years the surrogate strategy appears to be valid.

To test the limits of the surrogate probe method, we have begun examining the ^{67}Zn NMR spectroscopy of compounds where the Zn^{2+} sites are in a variety of coordination geometries. From a recent survey of zinc coordination in protein structures[5] it was shown that the Zn^{2+} metal sites are predominantly tetrahedral, with a fair number of pentacoordinated sites in these systems and some six-coordinate species. Those proteins that use zinc catalytically also tend to have water as at least one of the ligands. It is therefore of fundamental interest to understand the effects of water on the electronic environment of the zinc. It was shown in the previous cadmium work that water molecules had a strong deshielding effect on the metal. In fact, several single-crystal studies of cadmium-oxo compounds brought forth some correlations between shielding tensor elements and structure:[6] (i) tensor elements of like magnitude have similar orthogonal environments; (ii) the most deshielded element is aligned nearly orthogonal to planes containing water; (iii) if water oxygens are not present in the coordination sphere, then the least shielded element is oriented to maximize the shortest Cd−O shielding contributions; and (iv) the most shielded tensor element is nearly perpendicular to the longest Cd−O bond. The first two rules take an explicit understanding of the physics of the shielding interaction, namely it arises via a vector cross product between an angular momentum operator and coordinate vector. The last two rules relate the ability of

* Address correspondence to this author at Pacific Northwest National Laboratory: (e-mail) paul.ellis@pnl.gov; (phone) (509)372-3888; (fax) (509)376-2303.

† University of South Carolina.

(1) (a) Coleman, J. E.; Vallee, B. L. *J. Biol. Chem.* **1960**, *235*, 390. (b) Coleman, J. E.; Vallee, B. L. *J. Biol. Chem.* **1961**, *236*, 2244. (c) Lindskog, S. *J. Biol. Chem.* **1963**, *238*, 945. (d) Vallee, B. L.; Williams, R. J. P. *Proc. Natl. Acad. Sci.* **1968**, *59*, 498. (e) Latt, S. A.; Auld, D. S.; Vallee, B. L. *Proc. Natl. Acad. Sci.* **1970**, *67*, 1383.

(2) McAteer, K.; Lipton, A. S.; Ellis, P. D. Cadmium-113 NMR: A Surragate Probe for Zinc and Calcium in Proteins In *Encyclopedia of Nuclear Magnetic Resonance*; Grant, D. M., Harris, R. K., Eds.; John Wiley & Sons: New York, 1996; Vol. 2, pp 1085−1091 and reference cited within.

(3) (a) Armitage, I. M.; Pajer, R. T.; Schoot Uiterkamp, A. J. M.; Chlebowski, J. F.; Coleman, J. E. *J. Am. Chem. Soc.* **1976**, *98*, 5710. (b) Sudmeier, J. L.; Bell, S. J. *J. Am. Chem. Soc.* **1977**, *99*, 4499. (c) Otvos, J. D.; Armitage, I. M. *Biochemistry* **1980**, *19*, 4039. (d) Summers, M. F. *Coord. Chem. Rev.* **1988**, *86*, 43 and references therein.

(4) Kimblin, C.; Parkin, G. *Inorg. Chem.* **1996**, *35*, 6912−6913.

(5) Alberts, I. L.; Nadassy, K.; Wodak, S. J. *Protein Sci.* **1998**, *7*, 1700−1716.

(6) (a) Honkonen, R. S.; Doty, F. D.; Ellis, P. D. *J. Am. Chem. Soc.* **1983**, *105*, 4163. (b) Honkonen, R. S.; Marchetti, P. S.; Ellis, P. D. *J. Am. Chem. Soc.* **1986**, *108*, 912. (c) Marchetti, P. S.; Honkonen, R. S.; Ellis, P. D. *J. Magn. Reson.* **1987**, *71*, 294. (d) Kennedy, M. A.; Ellis, P. D. *J. Am. Chem. Soc.* **1990**, *29*, 541. (e) Kennedy, M. A.; Ellis, P. D.; Jakobsen, H. J. *Inorg. Chem.* **1990**, *29*, 550. (f) Rivera, E.; Ellis, P. D. *Inorg. Chem.* **1992**, *31*, 2096.

10.1021/ja011701e CCC: $22.00

oxygen ligands (other than water) to "direct" the projection of a component of the shielding tensor along a given bond axis. These empirical rules have been extended to other atoms bonded to cadmium, such as cadmium−sulfur or cadmium−selenium coordination systems by Santos et al.[7] and others.[8,9] In each case, the applicable paradigms have proven to be generalized to these other ligand systems.

Of particular interest was the ^{113}Cd single-crystal NMR study of cadmium formate dihydrate where there are two chemically distinct cadmiums per asymmetric unit.[10] One of the sites has the metal coordinated by a plane of four waters and two bridging formats, while the other cadmium site contains six bridging formates. Hence, the formates are good candidates to investigate the consequences of replacing neutral waters with charged ligands on the shielding and/or the quadrupole coupling tensors (for cadmium or zinc, respectively). As cadmium and zinc form isomorphous formates[11] one can make a direct comparison of the structural consequences of hydration on cadmium shielding and zinc quadrupole tensors. The quadrupole coupling constants have been determined for each site of zinc formate and found to be different, 9.5 and 6.1 MHz.[12] The challenge then is 2-fold, first to assign the electric field gradient (EFG) tensors to each site and then to orient the tensor in the molecule fixed frame of the zinc. In this work we present an X-ray crystal structure for zinc formate dihydrate, an assignment of the two sites using cross polarization and selective isotopic labeling, and a single-crystal NMR experiment determining the alignment of the EFG tensors in the crystal frame.

Experimental Section

X-ray Crystallography. Crystal data and details of data collection are given in Table 1. The crystal used in diffraction analysis was mounted inside a thin-walled glass capillary. Diffraction measurements were made on a Rigaku AFC6S automatic diffractometer by using graphite-monochromated Mo Kα radiation. The unit cell was determined from 15 randomly selected reflections obtained by using the AFC6 automatic search, center, index, and least-squares routines. All data processing was performed on a Silicon Graphics Indigo2 computer by using the TEXSAN structure solving program library obtained from the Molecular Structure Corp., The Woodlands, TX. Lorentz-polarization (Lp) corrections were applied. Neutral atom scattering factors were calculated by the standard procedures.[13a] Anomalous dispersion corrections were applied to all non-hydrogen atoms.[7b] An absorption correction (DIFABS) was applied. Full-matrix least-squares refinements minimized the function:

$$\sum_{hkl} w(|F_o| - |F_c|)^2$$

where $w = 1/\sigma(F)^2$ and $\sigma(F) = \sigma(F_o^2)/2F_o$, and

Table 1. Crystal Data for the Structural Analysis of Zinc Formate

formula	$Zn_2(HCO_2)_4(H_2O)_4$
formula weight	382.89
crystal system	monoclinic
lattice parameters	
a (Å)	8.703(2)
b (Å)	7.154(2)
c (Å)	9.315(2)
α (°)	90.0
β (°)	97.63(2)
γ (°)	90.0
V (Å^3)	574.9(2)
space group	$P2_1/c$ (no. 14)
Z (no. of molecules/unit cell)	2
Density (calc) (g/cm^3)	2.21
μ (Mo Kα) (cm^{-1})	4.23
temp of data collection (°C)	20
$2\Theta_{max}$ (deg)	55.0
no. observations used ($I > 3\sigma(I)$)	1081
no. of variables	94
max shift/error on final LS cycle	0.00
goodness of fit (GOF)*	1.26
residuals:[a] R; R_w	0.027; 0.057
absorption correction	difabs
largest peak in final diff. map (e$^-$/Å^3)	0.38

[a] $R = \sum_{hkl}(||F_{obs}| - |F_{calc}||/\sum_{hkl}|F_{obs}|$; $R_w = [\sum_{hkl} w(|F_{obs}| - |F_{calc}|^2)/\sum_{hkl} wF_{obs}^2]^{1/2}$, $w = 1/\sigma^2(F_{obs})$; GOF $= [\sum_{hkl}(|F_{obs}| - |F_{calc}|/\sigma(F_{obs})]/(n_{data} - n_{vari})$.

$$\sigma(F_o^2) = [\sigma(I_{raw})^2 + (0.02I_{net})^2]^{1/2}/\mathrm{Lp}$$

The crystallographic space group $P2_1/c$ was uniquely identified by the patterns of systematic absences observed during the collection ofintensity data. The structure was solved by a combination of direct methods (SIR92) and difference Fourier syntheses. All non-hydrogen atoms were refined with anisotropic thermal parameters. All hydrogen atoms were located. The formate hydrogen atoms were refined with isotropic thermal parameters. The hydrogen atoms on the water ligands were included in fixed positions.

Solid-State ^{67}Zn NMR. The samples utilized for NMR were labeled with ^{67}Zn at 88% (Cambridge Isotopes). The ^{67}Zn powder spectra were acquired at ambient temperature utilizing both a Varian Unity^{plus} spectrometer with a wide-bore Oxford Instruments magnet operating at 11.7 T (500 MHz for ^{1}H and 31.297 MHz for ^{67}Zn) and a Varian Unity^{Inova} spectrometer with a medium-bore (63 mm) Oxford Instruments magnet operating at 18.8 T (800 MHz for ^{1}H and 50.048 MHz for ^{67}Zn). The respective NMR probes used were a 5 mm Doty Scientific (DSI; Columbia, SC) wide-line probe and a home-built[14] 5 mm wide-line probe. The pulse sequences used were quadrupole echo (QE)[15] and cross polarization (CP)[16] combined with a quadrupole echo. Pulse widths for the DSI probe were 3 μs $\pi/2$ for ^{1}H during CP and a 3.4 μs π pulse, selective for the $\pm^1/_2$ transition for ^{67}Zn (5 μs nonselective, 1.7 μs selective $\pi/2$ pulse). The selective pulse widths used at 18.8 T were 1.8 and 3.6 μs, respectively, in a QE sequence. Single-crystal NMR measurements were made on the Unity^{plus} 500 spectrometer using a Doty Scientific single-crystal probe. The pulse sequence used was the QE sequence with selective pulse widths of 1.8 μs and 3.6 μs for the $\pi/2$ and π pulses, respectively. Analysis of the single-crystal data was performed with the program ASICS[17] and the high-field powder spectrum was analyzed with STARS[18,19] on a SUN Microsystems Ultra

(7) (a) Santos, R. A.; Gruff, E. S.; Koch, S. A.; Harbison, G. S. *J. Am. Chem. Soc.* **1990**, *112*, 9257. (b) Santos, R. A.; Gruff, E. S.; Koch, S. A.; Harbison, G. S. *J. Am. Chem. Soc.* **1991**, *113*, 469.
(8) Miner, V. W.; Prestegard, J. H. *J. Am. Chem. Soc.* **1985**, *107*, 2177.
(9) Sola, J.; González-Duarte, P.; Sanz, J.; Casals, I.; Alsina, T.; Sobrados, I.; Alvarez-Larena, A.; Piniella, J.; Solans, X. *J. Am. Chem. Soc.* **1993**, *115*, 10018.
(10) Honkonen, R. S.; Ellis, P. D. *J. Am. Chem. Soc.* **1984**, *106*, 5488.
(11) Osaki, K.; Nakai, Y.; Watanabe, T. *J. Phys. Soc. Jpn.* **1963**, *18*, 919.
(12) Larsen, F. H.; Lipton, A. S.; Jakobsen, H. J.; Nielsen, N. C.; Ellis, P. D. *J. Am. Chem. Soc.* **1999**, *121*, 3783−3784.
(13) (a) *International Tables for X-ray Crystallography*; Kynoch Press: Birmingham, England, 1975; Vol. IV, Table 2.2B, pp 99−101. (b) International Tables for X-ray Crystallography; Kynoch Press: Birmingham, England, 1975; Vol. IV, Table 2.3.1, pp 149−150.
(14) Sears, J. A.; Lipton, A. S.; Ellis, P. D. To be submitted for publication.
(15) (a) Solomon, I. *Phys. Rev.* **1958**, *110*, 61. (b) Davis, J. H.; Jeffrey, K. R.; Bloom, M.; Valic, M. I.; Higgs, T. P. *Chem. Phys. Lett.* **1976**, *42*, 390.
(16) Pines, A.; Gibby, M. G.; Waugh, J. S. *J. Chem. Phys.* **1972**, *56*, 1776.
(17) Vosegaard, T.; Hald, E.; Langer, V.; Skov, H. J.; Daugaard, P.; Bildsoe, H.; Jakobsen, H. J. *J. Magn. Reson.* **1998**, *135*, 126.
(18) Bildsoe, H. *Stars User's Guide. Spectrum Analysis of Rotating Solids*; Publication No. 87-195233-00, Rev A0296; Varian Associates Inc.: Palo Alto, CA, 1996.

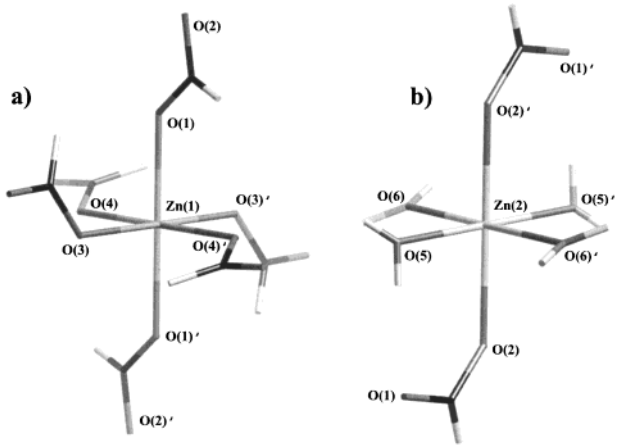

Figure 1. Structures of (a) the anhydrous site, Zn(1), and (b) the hydrated site, Zn(2), of zinc formate dihydrate. The primed atoms have been generated by symmetry.

Table 2. Selected Intramolecular Distances and Angles[a]

	Distances		
Zn(1)−O(1)	2.150(2)	Zn(2)−O(2)	2.166(2)
Zn(1)−O(3)	2.100(2)	Zn(2)−O(5)	2.102(2)
Zn(1)−O(4)	2.071(2)	Zn(2)−O(6)	2.052(2)
	Angles		
O(1)−Zn(1)−O(3)	87.31(6)	O(2)−Zn(2)−O(5)	88.73(6)
O(1)−Zn(1)−O(3)′	92.69(6)	O(2)−Zn(2)−O(5)′	91.27(6)
O(1)−Zn(1)−O(4)	87.27(6)	O(2)−Zn(2)−O(6)	89.78(9)
O(1)−Zn(1)−O(4)′	92.73(6)	O(2)−Zn(2)−O(6)′	90.22(9)
O(3)−Zn(1)−O(4)	89.50(6)	O(5)−Zn(2)−O(6)	89.28(7)
O(3)−Zn(1)−O(4)′	90.50(6)	O(5)−Zn(2)−O(6)′	90.72(7)

[a] Distances are in angstroms and angles are in degrees. Estimated standard deviations in the least significant figure are given in parentheses.

10 computer. All zinc chemical shifts are referenced with respect to 0.5 M $Zn(OAc)_2$ solution.

Results and Discussion

Solid-State Structure. The crystal lattice parameters of several monoclinic formate dihydrates (including zinc) were determined in 1963[11] and crystal structures for the magnesium and manganese salts were reported the following year.[20] The reported zinc structure was not refined and only an approximate structure obtained from a comparison of the intensities.[11] The two zinc atoms lie on crystallographic centers of symmetry. Figure 1 depicts the structures of each site with the numbering scheme to be used herein. Table 2 contains selected bond distances and angles from the present work for each of the respective zinc sites.

Both zincs have approximately octahedral coordination with an average cis angle of 90° (deviations not exceeding ±3°). Each site also has similar bond lengths with one each longer and shorter than the average of the Zn−O distances of each respective site, and the third unique bond length is almost equal to the average bond distance for that site. For each zinc the longest Zn−O bonds form the link between the two sites, Zn(1)−O(1) and Zn(2)−O(2).

Solid-State NMR. The two sites of zinc formate dihydrate have different quadrupole coupling values as one might expect due to the different coordination environments; however, the isotropic chemical shifts are nearly degenerate.[12] To determine which lineshape corresponded to which site we exploited the presence of water in the first coordination sphere of Zn(2) by using a combination of isotopic labeling (H_2O vs D_2O) and CP. First the contact time dependence of the magnetization was measured on the isotopically normal (^{67}Zn enriched) material. Then the sample was recrystallized repeatedly from D_2O, which effectively removed the proton source of the bound waters from the CP experiment, and the time dependent CP experiment was repeated. The results of the magnetization buildup from each sample are shown in Figure 2. The sharp feature at the left-hand side of the lineshape (marked by an asterisk), while present in both data sets, builds up rapidly to equilibrium in the protonated sample. This feature belongs to the broader of the two lineshapes ($Cq = 9.6$ MHz and $\eta_q = 0.45$) thereby implying that this zinc is the closest to the bound waters. Another piece of evidence supporting this is the relative ratios of the two lineshapes in each of the samples. In the hydrated material the broad lineshape is pronounced over the deuterated sample, which implies that it received more magnetization from the waters of hydration.

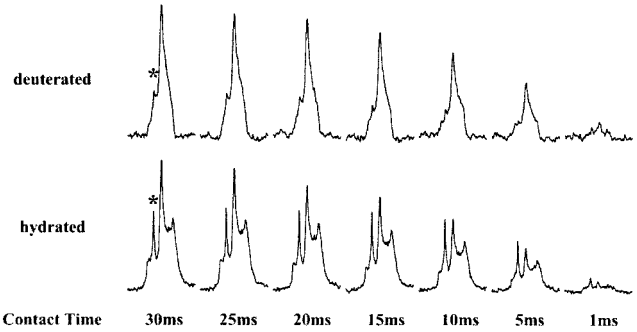

Figure 2. Static CP with varying contact time for hydrated and deuterated zinc formate dihydrate acquired at 11.7 T with a recycle delay of 5 s. The asterisk marks a feature present only in the broader lineshape.

Table 3. Quadrupole Coupling Parameters for Zinc Formate Dihydrate

site	δ_{iso}[a]	Cq (MHz)	η_q	ref
Zn(1)	−10 ± 5	6.05 ± 0.1	0.99 ± 0.1	12
Zn(1)	−27 ± 5	6.24 ± 0.05	0.93 ± 0.05	this work; 18.8 T
Zn(1)	−24 ± 7	6.34 ± 0.05	0.98 ± 0.01	this work; crystal
Zn(2)	0 ± 5	9.52 ± 0.1	0.62 ± 0.1	12
Zn(2)	−15 ± 5	9.58 ± 0.05	0.42 ± 0.05	this work; 18.8 T
Zn(2)	−26 ± 14	9.63 ± 0.06	0.45 ± 0.02	this work; crystal

[a] Chemical shifts are in ppm relative to 0.5 M $Zn(OAc)_2$.

The analysis of the single-crystal data provides additional values for the quadrupole coupling parameters for each site that are tabulated in Table 3.[21] Figure 3 shows the rotation plots for the *z*-axis of the goniometer with the respective fits for each site. The deviations from the experimental data can be attributed to the errors in the adjustments of the angles of the probe. The analysis of these data allows us to project the principal axis of the field gradient tensor back into the crystal frame. With the bond angles and distances for each site being similar one might expect that the field gradient tensors would be similar for each. However, the differences observed can be attributed to the characteristics of each type of ligand.

(19) Skibsted, J.; Nielsen, N. C.; Bildsoe, H.; Jakobsen, H. J. *J. Magn. Reson.* **1991**, *95*, 88.
(20) Osaki, K.; Nakai, Y.; Watanabe, T. *J. Phys. Soc. Jpn.* **1964**, *19*, 717.

(21) The inclusion of chemical shift anisotropy parameters was not needed in the fit of the data.

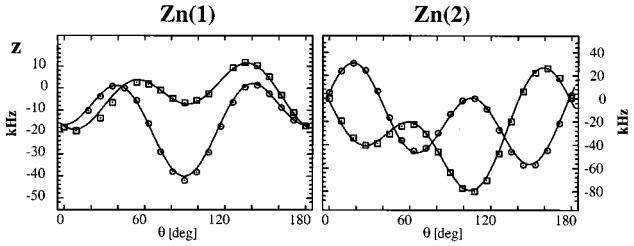

Figure 3. Single-crystal rotation plots for the *z*-axis of the goniometer and their respective fits of each set of data. Data points were taken from 0 to 180° in 9° increments.

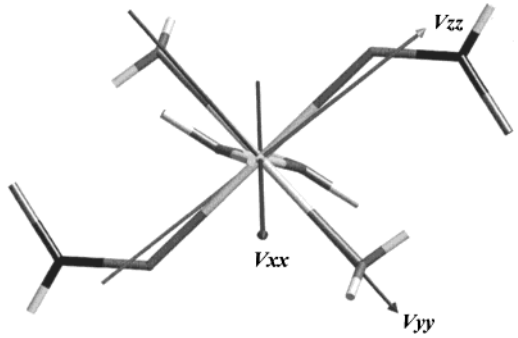

Figure 4. Principal elements of the field gradient tensor plotted onto the molecular frame for the hydrated site. The V_{zz} element is nearly orthogonal to the plane containing the water oxygens.

For the hydrated site (Zn(2)), with the four waters around the metal, the V_{zz} element of the tensor was determined to lie along the vector made by the axial formyl groups. As stated earlier this corresponds to the longest Zn−O bond (2.166 Å) for this site and this vector is nearly orthogonal to the plane containing waters. Consequently both the V_{xx} and V_{yy} elements lie nearly in the plane of the waters. The tensor element with the next largest magnitude, the V_{xx} component, is 30° from the shortest Zn−O bond (2.052 Å). The orientation is plotted onto the molecular frame in Figure 4.

The anhydrous site (Zn(1)), which has the six bridging formates, also has the V_{zz} element aligned nearly along a Zn−O_{formyl} vector. However, for this site the vector is roughly 16° from the Zn−O(4) bond, the shortest of the three at 2.071 Å. This is in the *bc* plane (orthogonal to the *a** axis) which consists of a sheet of bridging formates. The tensor element with the next largest magnitude, V_{xx}, is aligned near the longest Zn−O bond, 2.150 Å. This element also lies in the plane formed by O(1)−O(3)−O(1)′−O(3)′. Depicted in Figure 5 is a view of the sheets made up of several unit cells. One can see the formate sheets (the polyhedra) separated by the planes of hydrated columns.

Examining both of these sites one might ask two questions: if each site has all oxygens in the primary coordination sphere with similar bond lengths, then why are the quadrupole coupling parameters not similar; second, if there are four waters or four bridging formyl groups in a plane around the metal, why are the bond lengths within each plane so different? The first point is easily understood as the consequence of ligation of the neutral water species versus the charged formates. From the ^{113}Cd data we know the most shielded element is oriented to maximize the contribution from the longest Cd−O bond. Furthermore, water is a stronger deshielding ligand than the formate anion as the most deshielded element is oriented normal to the plane of the waters.[10] From this we can assume that the hydrated metal

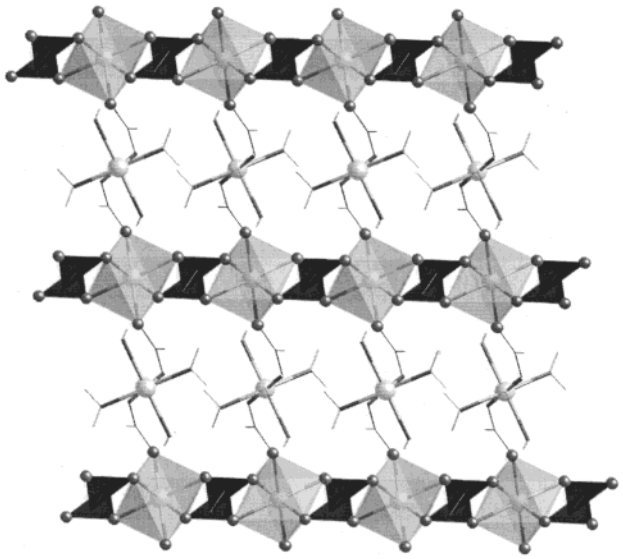

Figure 5. View of the polymeric lattice of zinc formate dihydrate with polyhedra on the anhydrous sites. The planes formed by the water oxygens are nearly in the plane of the paper.

center (for both cadmium and zinc) carries a slightly higher positive charge than the anhydrous site. This in turn would contribute to the stronger electric field gradient on the zinc for the hydrated site.

An approximate view of the quadrupole coupling constant has been provided by Slichter.[22] In this treatment, the V_{zz} element of the field gradient (and therefore Cq) is directly proportional to $1/r^3$ and electronic charges (both internal and external). This relation results in the sensitivity of Cq to charges that are closer to the nucleus. Qualitatively, one can say that for two differently charged nuclei each with identical point charges (of opposite sign to the atom) an equal distance from the nucleus will have different Cq values. Further, the site with the larger charge differential for the same distance will have the larger field gradient. This sensitivity of Cq to local charges can be utilized to study bond hybridization or the degree of covalency.[23] However, in this case even though the Zn−O bond distances are similar between the sites, it is difficult to rationalize the larger Cq of Zn(2) due to charges alone.

To address the second question of why are the same ligands within the plane of each site are different, we can again refer back to the cadmium analogue.[24] It was observed that the polymeric structure is supported by an extensive network of hydrogen bonds. We note here that a similar network exists for the zinc structure. Each water has a hydrogen bond to a formate group and likewise each formate oxygen participates in a hydrogen bond. The distances are given in Table 4. From the table one can see that the strongest hydrogen bond (as reflected by the shorter distances) exists to the bridging formate oxygen of the hydrated site. Presumably due to steric constraints this and the other oxygen of this group (which bonds to the other zinc) represent the longest Zn−O bonds in the molecule. The next strongest hydrogen bond also originates from the same water molecule. This has the effect of weakening the formal bonds between the water oxygen and its hydrogens (see Table

(22) Slichter, C. P. *Principles of Magnetic Resonance*, 3rd ed.; Springer-Verlag: New York, 1978, 1990; Chapter 10.
(23) Dailey, B. P.; Townes, C. H. *J. Chem. Phys.* **1955**, *23*, 118.
(24) Post, M. L.; Trotter, J. *Acta Crystallogr.* **1974**, *B30*, 1880.

Table 4. Hydrogen Bond Distances (Å)[a]

Zn(2)−O(5)−H(3)	0.67	H(3)···O(4^{ii})	2.15
Zn(2)−O(5)−H(4)	0.76	H(4)···O(1)	1.99
Zn(2)−O(6)−H(5)	0.93	H(5)···O(2^{iii})	1.86
Zn(2)−O(6)−H(6)	0.85	H(6)···O(3^{ii})	1.95

[a] Superscipts refer to the symmetry-related positions: (*i*) x, $^1/_2 - y$, $^1/_2 + z$; (*ii*) x, $1 + y$, z; (*iii*) $1 - x$, $^1/_2 + y$, $^1/_2 - z$.

4), thereby strengthening its bond to the metal. Concomitantly, the other oxygen on this bridging formyl group also has a long Zn−O bond and a strong hydrogen bond from another water molecule. However, the second hydrogen from this water has a weak hydrogen bond to one of the formyl groups of the sheet (again presumably due to steric interactions) that does weaken the formate oxygen's bond to the metal differentiating it from the other bridging group making up the sheet structure.

An analogous hydrogen bonding network also exists for zinc acetate dihydrate where the waters connect adjacent molecules along the *b* and *c* axes to form sheet structures.[25] From a recent ^{67}Zn single-crystal NMR study we know that the largest two components of the EFG tensor lie in the *bc* plane nearly along each crystallographic axis.[26] From this same work the V_{zz} component is nearly orthogonal to the plane made by the "equatorial" acetate oxygens, while the V_{xx} element bisects the angle made by the waters and the zinc. While this structure is more distorted relative to either of the two zinc formate sites, the quadrupole coupling is lower here than for either of the formates.[26,27] This results from the uniformly longer Zn−O bonds present in the acetate.

Also noted in the crystal study of zinc acetate dihydrate was a modest shielding anisotropy that was not detected in the powder lineshapes. The absence of shielding anisotropy in the formate lineshapes was confirmed with a QE experiment at high field, 18.8 T. Figure 6 depicts the resulting experimental and simulated data. The contribution to the lineshapes from the quadrupole coupling decreases as the field increases while the CSA contribution increases. The fact that the overlapping lineshapes can be simulated by using only the quadrupole contribution at this field means that any CSA present has to be smaller than our detection limits even at this field (<30 ppm).

Conclusion

The respective quadrupole coupling parameters have been assigned to each site of zinc formate dihydrate. The structure has been determined including all hydrogen positions, and the electric field gradient tensor elements have been oriented into the crystal frame. In much the same way as the cadmium single crystal work facilitated correlations between NMR parameters and structure, we can begin to see that there are going to be trends by which we may predict quadrupole tensor orientations. For instance it appears that the V_{zz} component will be nearly orthogonal to planes containing water. Also if water is not present in the first coordination sphere then V_{zz} will be oriented along the shortest Zn−O bond. Clearly more single crystal work is necessary to further support these tentative conclusions as well as to determine the consequences of other heteroatoms in the primary coordination sphere.

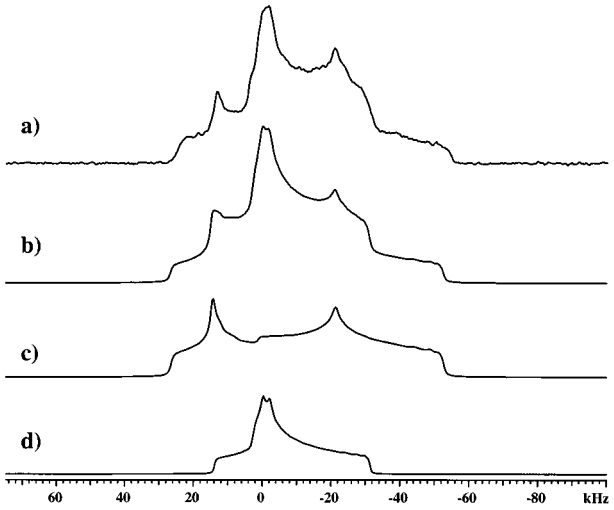

Figure 6. Experimental (a) and simulated (b−d) powder lineshapes of zinc formate dihydrate. Data acquired at 18.8 T using 1.8 and 3.6 μs selective $\pi/2$ and π pulses respectively and a 1s recycle delay. Simulation parameters are listed in Table 4. Spectra c and d are the individual lineshapes for Zn-(2) and Zn(1), respectively.

Finally, the existence of the extensive hydrogen bonding network in the formate structure has limited our ability to perform ab initio calculations of the EFG tensor for each site. The predicted values for the EFG tensor elements did not show evidence for convergence until we had formed structures containing the equivalent of three or more unit cells. At this point the calculation started to approach heroic proportions and we elected not to attempt further calculations. It is clear the role of the waters and their degree of hydrogen bonding are critical in these calculations.

Acknowledgment. This work was supported by a grant from the National Institutes of Health (Federal Grant GM-26295). The NMR experiments were carried out in the Environmental Molecular Sciences Laboratory (a national scientific user facility sponsored by the Department of Energy Office of Biological and Environmental Research) located at Pacific Northwest National Laboratory and operated for DOE by Battelle.

Supporting Information Available: Tables of positional parameters, intramolecular distances, and intramolecular bond angles for zinc formate dihydrate, $Zn_2(HCO_2)_4(H_2O)_4$, and single-crystal NMR rotation plots for all three goniometer axes with their respective fits (PDF); X-ray crystallographic data of zinc formate dihydrate (CIF). This material is available free of charge via the Internet at http://pubs.acs.org.

JA011701E

(25) Van Niekerk, J. N.; Schoening, F. R. L.; Talbot, J. H. *Acta Crystallogr.* **1953**, *6*, 720.
(26) Vosegaard, T.; Andersen, U.; Jakobsen, H. J. *J. Am. Chem. Soc.* **1999**, *121*, 1970.
(27) Kunwar, A. C.; Turner, G. L.; Oldfield, E. *J. Magn. Reson.* **1986**, *69*, 124.